DOI: 10.15480/882.9296

Eighth International Symposium on Marine Propulsors
smp'24, Berlin, Germany, March 2024

Uncertainty Quantification of RANSE and BEM models for Hydrodynamic Performance of Supercavitating Hydrofoils

Surabhi Srivastava[1], Stefano Brizzolara[1], Nicholas Husser[2],

[1]Kevin T. Crofton Department of Aerospace and Ocean Engineering, Virginia Tech, Blacksburg, VA, USA
[2]Yamaha Motor Corporation, Atlanta, GA, USA

ABSTRACT

Innovating, testing, and design of supercavitating propellers and hydrofoils used in high-speed marine crafts can be time consuming and expensive. Various numerical methods and Computational Fluid Dynamics (CFD) models can help in the design and optimization processes and hence improve the efficiency of the production pipeline. This study explores the capabilities of Unsteady RANSE based CFD simulations and a potential based, low order, 2D Boundary Element Method (BEM) in predicting the performance and cavitation patterns for a 2D supercavitating hydrofoil. The goal of this study is to quantify the uncertainty in these performance prediction approaches by validating their results against available experimental data. The study revealed that unsteady RANSE, using the $k-\omega$ turbulence model and the full Rayleigh-Plesset cavitation model predicts the most accurate hydrodynamic performance parameters. However, the most accurate cavitation patterns were predicted using the $k-\epsilon$ turbulence model and the Schnerr-Sauer cavitation model. The low order BEM also showed results that agreed well with the experimental data, especially considering the approximation of the model. A further investigation on the influence of control parameter in CFD simulations showed that seed density and seed diameter can have significant influence on the cavitation pattern prediction.

Keywords

Supercavitation, Propellers, CFD, BEM, Uncertainty quantification

1 INTRODUCTION

Over the last few years, there has been a large increase in the demand for outboard engines for high-speed marine crafts. To minimize the weight and size of engines, propellers must rotate fast while advancing at high speeds. Conventional propellers are adversely affected in such cases due to cavitation. Cavitation is a phenomenon which occurs when the pressure on the surface drops below the vapor pressure of the operating fluid causing the fluid to vaporize and form bubbles at the blade surface. This can structurally damage the propellers, cause noise, and affect performance. Propellers on high-speed marine crafts operate in the supercavitating (SC) regime, a condition where the cavitation bubble is longer than the chord length of the propeller section. With the increasing maximum power of outboard engines resulting from technological advancements, there is a need to design new, high performance super-cavitating propellers (SCP) which can deliver large thrust at high speeds with limited maximum size. Innovative designs can only come from innovative super-cavitating hydrofoils (SCHs) that can be designed by numerical hydrodynamic simulation methods (Vernengo et al. 2016).

Efforts to computationally predict the performance of SCHs and SCPs have persisted for a very long time. Tulin (1962) summarizes some of the early methods used in cavitating flow predictions. These approaches include different lifting surface methods which relied on the linear cavity theory that was applicable to only thin SCP and SCH sections. However, inaccurate outputs were obtained when this numerical approach was implemented to propeller sections with large thickness values and rounded leading edges (Fine and Kinnas 1993). Moreover, these methods relied on multiple assumptions and empirical corrections (Young and Kinnas 2003). During the 1990s, the PROPCAV method was developed (Kinnas and Fine 1992, Fine and Kinnas 1993), which is a low-order, potential based BEM. It is nonlinear in nature such that for a known cavitation number, the cavity extent and location is unknown. It is an iterative method that can predict steady partial and supercavitation for SCPs and SCHs for conventional propellers. Further developments by Young and Kinnas (2003) adapted this method for cavitation prediction of SCHs and SCPs with truncated trailing edges (TE). Additionally, they validated their method using experimental data from Matsuda et al. (1994).

Table 1. CFD Flow and Cavitation Model Test Matrix. Green shaded cells with '✓' indicate tested model combinations and grey shaded cells with '×' indicate models that were not tested.

		Flow Models				
Cavitation Model		$k-\epsilon$ Turbulence Model		$k-\omega$ Turbulence Model		Laminar
		Turbulent flow	Transitional flow	Turbulent flow	Transitional flow	
	Schnerr-Sauer	✓	✓	✓	✓	✓
	Full Rayleigh Plesset	✓	×	✓	×	×

Recent advancements in Computational Fluid Dynamics (CFD) and various numerical methods have provided a means to predict propeller performance in cavitating conditions with increased accuracy. Unsteady RANSE based solvers with cavitation models can simulate realistic operating conditions. The use of these methods on SC sections are still being explored (Vernengo et al. 2016, Gaggero & Brizzolara 2009). Such studies have also led to the advancement of the BEM for SC profiles (Gaggero & Brizzolara 2009) in addition to alternative BEM by Fine & Kinnas (1993) and Young & Kinnas (2003). An important motivation for the continued development of potential flow based numerical methods is their computational efficiency. Despite the accuracy of unsteady RANSE, in this study, a 2D simulation required over 200 processors and approximately 2.5 days of time, whereas the potential flow-based method required only 1 processor and was complete in approximately 15 seconds.

The goal of this study is to contribute to the exploration of the scope of supercavitating flow prediction using unsteady RANSE solvers and numerical methods. Here, the capabilities of various models to simulate 2D supercavitating flows are systematically explored. The performance and cavitation pattern predictions from the BEM and the unsteady RANSE models are compared against experimental data. It is important to note that due to the limited availability of recent experimental performance data on 2D SCHs and SCPs, the results of this article are validated against data from Parkin (1956) for a 2D SCH section seen in Figure 1. The RANSE models explored include different cavitation, turbulence, and transitional models. The uncertainty regarding the performance predictions of each approach is quantified by numerically validating them against the available experimental data. Furthermore, the cavitation pattern predictions are also qualitatively compared.

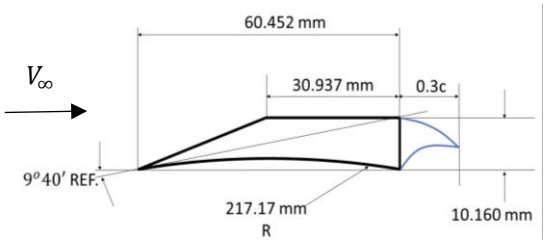

Figure 1. Circular Arc Hydrofoil from Parkin (1956) with the closing zone of 0.3c at the truncated trailing edge seen in blue.

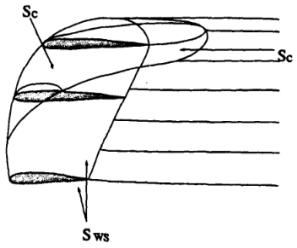

Figure 2. Taken from Fine (1992). The schematic shows the cavitating foil and wake regions S_C and the wetted surface S_{WS}.

2 COMPUTATIONAL FLUID DYNAMICS (CFD) MODELS

The 2D performance prediction capabilities of a range of turbulence and cavitation models are assessed in Siemens Star-CCM+. The simulations are based on the Reynolds Averaged Navier Stokes Equations (RANSE). Turbulence is modeled using either the $k-\epsilon$or the $k-\omega$ turbulence models. Transitional flow is modeled using turbulence suppression and a γ transition model depending on the selected turbulence model. The flow is also simulated to be laminar in nature. Lastly, cavitation is simulated using either the Schnerr-Sauer or Full Rayleigh-Plesset model. The turbulence models were paired with either of the cavitation models. Table 1 documents the different combinations of these models that were tested to assess the performance of a 2D SCH. The flow is solved using an implicit unsteady solver with a time step of 10^{-5}s and for a physical time of 2 seconds where each time step has 5 iterations.

3 2D BOUNDARY ELEMENT METHOD (BEM)

The potential flow based numerical method used in this study is a 2D BEM from Gaggero and Brizzolara (2008) and Vernengo et al. (2016). It is based on PROPCAV (Kinnas and Fine 1992) but modified for supercavitating geometries with truncated trailing edges (Young 2002). Assuming a uniform, potential flow and a uniform distribution of point sources and dipoles on the hydrofoil surface and wake, the perturbation potential at every arbitrary point p on the combined wetted and cavitating surface of the hydrofoil must satisfy Green's 3rd identity:

$$2\pi\phi_p = \int_{S_{WS}\cup S_c}\left[\phi_p\frac{\partial G_{pq}}{\partial n_q} - G_{pq}\frac{\partial \phi_q}{\partial n_q}\right]dS + \int_{S_W}\left[\Delta\phi_w\frac{\partial G_{pq}}{\partial n_q}\right]dS \quad (1)$$

Where q is a different arbitrary point on the hydrofoil or the wake, $G = 1/r_{pq}$ is the Green's function equal to the

inverse of the distance between points p and q, and n is the unit normal vector to the surface. The different regions over which this integral is performed include the wetted surface, cavitating surface, and the cavitating wake region abbreviated as S_{WS}, S_C, and S_W, respectively. These are observed in Figure 2. To solve for the unknown potentials on the hydrofoil and in the wake, a range of kinematic and dynamic boundary conditions are used.

The problem is set up such that by using various boundary conditions, only a single parameter is unknown in each region. The dipole strengths are unknown in the wetted regions and the source strengths are unknown in the cavitating regions. The unknowns are numerically solved for using Eq. (1) and the boundary conditions through a system of equations. This process is iteratively performed to obtain a converged solution, building upon the solution from previous iterations. Details regarding the theoretical implementation and numerical algorithm are present in Fine (1992), Young (2002), and Gaggero and Brizzolara (2008). It is important to note that this method assumes inviscid, incompressible, and irrotational flow. Additionally, for this study, the cavitation bubble extent in the wake is not computed.

4 EXPERIMENTAL SET UP

Experimental data from Parkin (1956) is used for the uncertainty quantification in the CFD and BEM results. The cavitation and performance data from the 2D Circular Arc Hydrofoil geometry, as seen in Fig. 1, is used to validate the performance predictions from the unsteady RANSE models and the BEM. The experiment was conducted in a "nearly rectangular" test section which was 35.6 cm high and 7.62 cm wide. The hydrofoil used in these experiments was placed horizontally in the test section spanning the entire tunnel width with a small clearance near the walls resulting in two-dimensional flow. Performance data was measured over an extensive range of inflow velocities and angles of attack. The cavitation number, defined in Eq. (2), was calculated either by measuring p_{vap} in the cavitation bubble (σ_k) or by assuming a theoretical vapor pressure value (σ_v). The latter was performed when the cavitation bubble was unsteady.

$$\sigma = \frac{(\rho g h + p_{atm}) - p_{vap}}{\frac{1}{2}\rho v^2} \qquad (2)$$

The test conditions considered for the performance prediction methods include $0.2 < \sigma < 1.1$ and $0^o \leq \alpha \leq 10^o$. Each performance prediction approach was customized to best simulate the operating conditions of the hydrofoil. This is described in the following subsections.

4.1 2D BEM Set Up

Since the geometry being considered is a supercavitating hydrofoil with a truncated TE, a temporary closing zone is implemented to account for the "openness" of the TE. This has negligible influence on the solution if the closing zone is within the separation bubble and its TE point is aligned with the selected wake sheet (Young 2002). The closing zone is 30% of the chord length and the total number of points of the geometry surface was 241 with 41 points on the face and back of the closing zone. This is seen in Figure 1. This point distribution was selected after a performance parameter convergence was obtained in a grid sensitivity study. Where possible, the experimental σ calculated by measuring p_{vap} in the cavitation bubble was specified to predict the performance of the hydrofoil. In other cases, the σ based on freestream static pressure was utilized.

4.2 Unsteady RANSE Simulation Set Up

The 2D Circular Arc hydrofoil is modeled in a 5 x 2 m fluid domain. A Polygonal and Prism Layer mesh is used. The base size is kept constant at 0.02 m with a target surface size of 32% of the base size. The minimum surface size was 1% of the base size. There are 32 prism layers around the hydrofoil to solve for the boundary layer and the prism layer thickness is kept constant at 2.56 cm. The prism layer thickness is gradually reduced at the sharp vertices of the hydrofoil as can be seen in Figure 3. This ensures that the mesh cells do not increase in size due to large changes in angles of the foil surface. Lastly, the wake is refined with a mesh size of 1% of the base size.

The flow is modeled to be a multiphase flow with the two phases being water and vapor. It is simulated using a range of turbulence and cavitation models as listed in Table 1. The vapor pressure for the fluid is assumed to be 2300 Pa. The velocity is kept constant at 11.26 m/s and the flow σ is varied by changing p_0. Due to the nature of the turbulence and cavitation models used, the flow σ value is

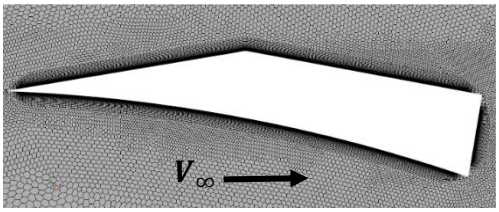

Figure 3. 0.02 m base mesh size, AoA = 10^o, 32 prism layers around the hydrofoil surface. Inflow velocity is from left to right.

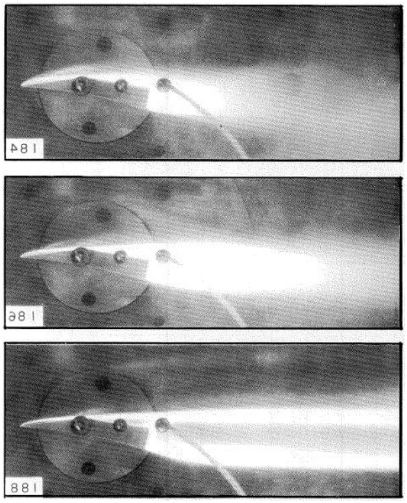

Figure 4. Taken from Parkin (1956). AoA = 10^o, from top to bottom, $\sigma_v = 0.792, 0.444$, and 0.264. Image horizontally flipped. Inflow velocity is from left to right.

equated to σ_v. The cavitation bubble is predicted by creating an isosurface for a volume fraction of vapor > 0.5 as observed in Figures 6 and 9.

4.3 Test Conditions

The performance capabilities of BEM and CFD are tested through different studies to quantify the uncertainty between their performance prediction capabilities and the performance data from Parkin (1956). It is important to note that the physics being modelled in this type of flow is very complex. Not only are there two phases of the fluid, but there are multiple forms of cavitation patterns. Supercavitation occurs at low σ values. As σ increases, partial cavitation occurs which is often unsteady. The cavitation bubble itself fluctuates in length and sheds bubbles into the wake. Moreover, cavitation can occur on the back, on the face, and in the separated region of the truncated trailing edge. This change in cavitation pattern can be observed in Figure 4. For this reason, the first section of the study focuses on comparing the performance predictions of the BEM and various unsteady RANSE models to the experimental data for varying cavitation numbers. This is done for 2 angles of attacks, 0^o and 10^o, and cavitation numbers ranging from 0.2 to 1.1. These two angles of attack are particularly chosen as Parkin (1956) provides real time images for them.

The predicted performance parameters are also compared to the experimental data for varying angles of attack at σ values of 0.26 ± 0.02, 0.43 ± 0.02, and 0.64 ± 0.08. The uncertainty in the cavitation number accounts for the difference in flow conditions when the hydrofoil angle of attack was changed. This study is done for unsteady RANSE models with laminar flow, $k-\omega$ turbulence with full Rayleigh-Plesset cavitation model, and $k-\epsilon$ turbulence model with Schnerr-Sauer cavitation model. The angles of attack included in this study are $0^o, 2^o, 4^o, 8^o,$ and 10^o. These conditions were also tested using the BEM.

Following this, a deeper investigation on the influence of the cavitation model control parameters on the resolved cavitating flow is conducted. The seed density and seed diameters were varied for the $k-\omega$ turbulence model with full Rayleigh-Plesset cavitation model and $k-\epsilon$ turbulence model with Schnerr-Sauer cavitation model. This study compares the predicted performance parameters and the cavitation extent with the experimental data. The cavitation number is kept constant at 0.444 and a fixed angle of attack of 10^o is used.

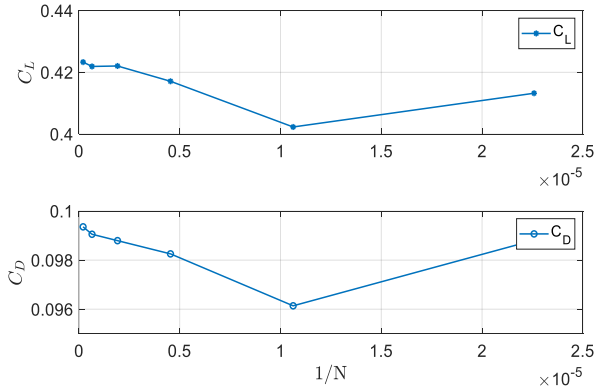

Figure 5. Variation in mean performance parameters for different mesh coarseness levels. AoA = 10^o and $\sigma = 0.264$

5 MESH SENSITIVITY STUDY

A mesh sensitivity study was performed to evaluate the influence of cell density on the obtained solution. The study is conducted for $AoA = 10^o$ and $\sigma = 0.264$. The physics models used in these simulations are kept constant and include the $k-\epsilon$ turbulence model with the Schnerr-Sauer cavitation model. A polygonal mesher and a prism layer mesher are used. The number of prism layers and prism layer thickness are kept constant at 32 and 2.56 cm (0.42c), respectively. The mesh base size, normalized by chord length, varies to 0.17c, 0.33c, 0.66c, 1.32c, 2.65c, and 5.29c (0.01, 0.02m, 0.04m, 0.08m, 0.16m, and 0.32m).

Figure 5 shows the variation in the mean C_L and C_D with varying mesh distributions. The vertical axis indicates the performance parameters, and the horizontal axis shows 1/N where N is the number of cells in the mesh. With increasing cell density, the performance parameters are seen to converge with some very minor fluctuations at base size of 0.01 m. These small fluctuations can be attributed to the small changes in forces that are captured due to the intricate mesh. As the mesh becomes coarser, the fluctuations in the mean forces amplify. The influence of the mesh on the cavitation bubble extent can be seen in Figure 6. As the base size decreases, more features are observed in the cavitation pattern. At the largest base size, 0.32 m, the cavitation bubble is seen detaching on the back and the face. However, unlike other predicted cavitation patterns, it has a smooth, closed bubble trailing edge. At a base size of 0.08 m, the cavitation bubble TE is seen to have a non-zero thickness. At a base size of 0.04 m, the cavitation bubble also shows bubbles being shed into the wake. Additionally, partial cavitation is also observed at the LE of the hydrofoil.

These trends indicate that as the base size decreases, the overall shape of the cavitation bubble converges. Additionally, smaller bases sizes also reveal partial cavitation which is overlooked in coarser meshes. Lastly, while the overall shape of the cavitation bubble is predicted by each mesh distribution, the trailing edge of the bubble varies in each of them. This indicates that the bubble becomes unsteady and fluctuates at its trailing edge. The

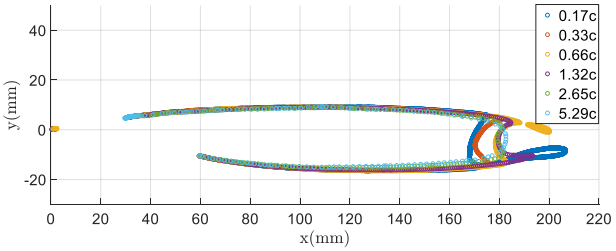

Figure 6. Influence of mesh coarseness levels on cavitation pattern predictions. AoA = 10^o and $\sigma = 0.264$

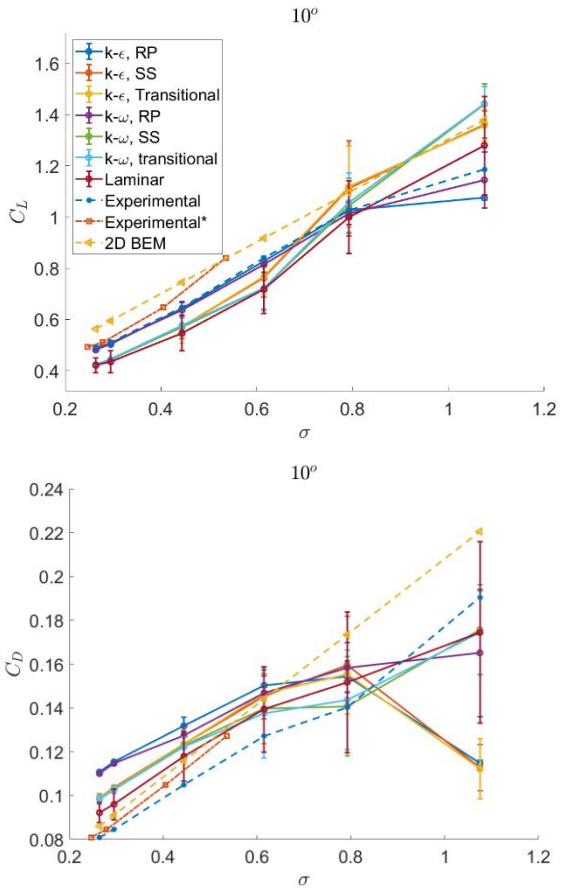

Figure 7. AoA = 10^o, Performance prediction capabilities of the BEM and various CFD models. Validated against 'Experimental (σ_v)' and 'Experimental*', data. Top (a): C_L v.s. σ. Bottom (b): C_D v.s. σ

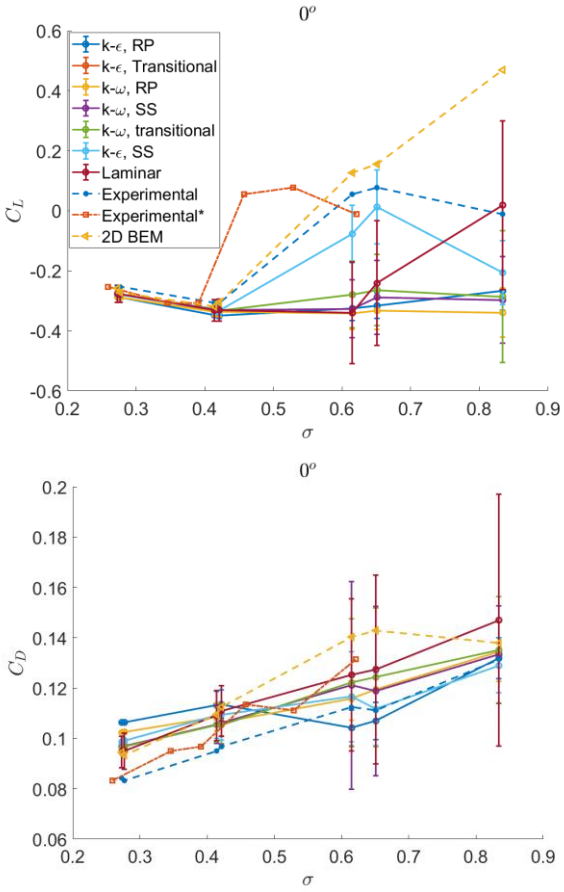

Figure 8. AoA = 0^o, Performance prediction capabilities of the BEM and various CFD models. Validated against 'Experimental (σ_v)' and 'Experimental*', data. Top (a): C_L v.s. σ. Bottom (b): C_D v.s. σ

following analyses were conducted using a base size of 0.02 m.

6 INFLUENCE OF σ ON PERFORMANCE PARAMETERS

The influence of varying σ on the performance parameters predicted through different approaches is analyzed and validated against the experimental data from Parkin (1956). The angles of attack considered are 0^o and 10^o. The combinations of the physics models simulated are documented in Table 1. In addition to the different unsteady RANSE simulations, the performance prediction results from the BEM were also validated.

6.1 At AoA = 10^o

Figures 7 (a) and (b) compare the mean C_L and C_D predicted from the different unsteady RANSE and numerical approaches to the experimental data at AoA = 10^o. The cavitation number ranged between 0.26 to 1.1 and is shown on the horizontal axis. In the figures, the performance parameters are seen on the vertical axis. The experimental data is shown as orange and blue dot-dashed lines with '*' and square markers. The blue dashed "Experimental" curve uses σ_v which is based on a theoretical vapor pressure and the orange dash-dot "Experimental*" curve uses σ_k which is based on the pressure measured inside the cavitation bubble. Note that the orange curve does not extend over the entire σ range as at higher σ values the pressure in the cavitation bubble was too unsteady to measure.

Figure 7 (a) shows that the simulation using the $k-\omega$ turbulence model with full Rayleigh-Plesset cavitation model simulation most accurately predicts C_L throughout varying cavitation numbers, underestimating by 3.5% at the largest σ value. There is a very close overlap observed at low cavitation numbers and the experimental data falls within the uncertainty of the unsteady RANSE data at higher cavitation numbers. This is also seen in the $k-\epsilon$, full Rayleigh-Plesset model simulation for $0.264 \leq \sigma \leq 0.8$. Other models underpredicted C_L. At low σ values, the underestimation is almost constant throughout the different models. However, as σ increases, the models fail to follow the general trend observed in the experimental data. Lastly, the uncertainty in the performance parameters is found to be higher at large cavitation numbers due to the presence of unsteady, fluctuating cavitation patterns as observed in Figures 9, 11, and 12.

On the other hand, despite being a low order method, the BEM is seen to follow the same general trend as observed in the experimental data. There is almost a constant difference between the experimental C_L and the BEM predicted C_L. The percentage difference between the two data sets ranged between 6.8% and 16.4%.

Figure 7 (b) shows the C_D predictions of the different CFD simulations and the BEM compared to the experimental data. Unlike the trends observed in Figure 7 (a), the most accurate performance predictions at low σ values are made using the low order BEM. Additionally, the 2D BEM is found to be the only method to follow the general trend observed in the experimental C_D data. All unsteady RANSE models, on the other hand, overpredicted the hydrofoil C_D significantly, including the ones with the full Rayleigh-Plesset models which showed the best agreement with the C_L experimental data. Additionally, all unsteady RANSE simulations fail to capture the general trend of C_D as σ increases.

6.2 At $AoA = 0^o$

Figure 8 (a) and (b) compare the mean C_L and C_D predicted from the different unsteady RANSE and numerical approaches to the experimental data at AoA = 0^o. Compared to 10^o, a 0^o angle of attack is unrealistic as it leads to zero or negative lift. Nonetheless, this angle of attack was considered to test the capabilities of the different performance prediction methods for difficult flow conditions. Figure 8 (a) shows the variation in C_L with respect to σ. At low cavitation numbers, all performance prediction methods agree well with the experimental data, especially the C_L data from the BEM. When $0.4 < \sigma < 0.6$, most unsteady RANSE models collapse and diverge from the general trend of the experimental data. Only the BEM results and the unsteady RANSE simulations with $k-\epsilon$ turbulence model and Schnerr-Sauer cavitation model data follow the general trend. These too diverge from the experimental data at $\sigma \geq 0.65$.

Figure 8 (b) shows the variation in C_D with respect to the varying cavitation number. All prediction methods are seen to follow the general trend of the experimental data. However, the predicted C_D values are not accurate. This is similar to the trend observed for 10^o angle of attack.

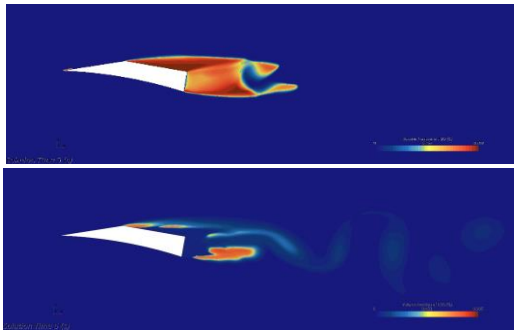

Figure 9. Instantaneous cavitation pattern indicated through a volume fraction of vapor ≥ 0.5. The red regions show vapor, and the blue regions show water. $\sigma = 0.444$ and AoA = 10^o. (a) Top: Cavitation pattern using the $k-\epsilon$ turbulence model and the Schnerr-Sauer cavitation model. (b) Bottom: Cavitation pattern using the $k-\omega$ turbulence model and the full Rayleigh-Plesset cavitation model.

In addition to comparing the predicted performance parameters against the experimental data, the cavitation pattern predicted through the various unsteady RANSE models were also qualitatively compared with the experimental images. At $\sigma = 0.444$ and $\alpha = 10^o$, the unsteady RANSE simulation using the $k-\epsilon$ turbulence model and the Schnerr-Sauer cavitation model predicted the most accurate cavitation pattern despite its inaccurate performance parameter predictions. This is observed in Figure 9 (a) and compared to Fig. 4. Additionally, Fig. 9 (b) shows the cavitation pattern predicted by the simulation using the $k-\omega$ turbulence model and the full Rayleigh-Plesset cavitation model. As is observed, the cavitation pattern predicted is inaccurate despite the accurate performance prediction parameters obtained. It is important to note that in both simulations, the number of seeds in the fluid and the seed diameter were kept constant at 10^{12} and 10^{-6} m, respectively.

7 INFLUENCES OF AoA ON PERFORMANCE PARAMETERS

To investigate the influence of the angle of attack on the performance parameter predictions, three cavitation conditions were chosen. The cavitation numbers were

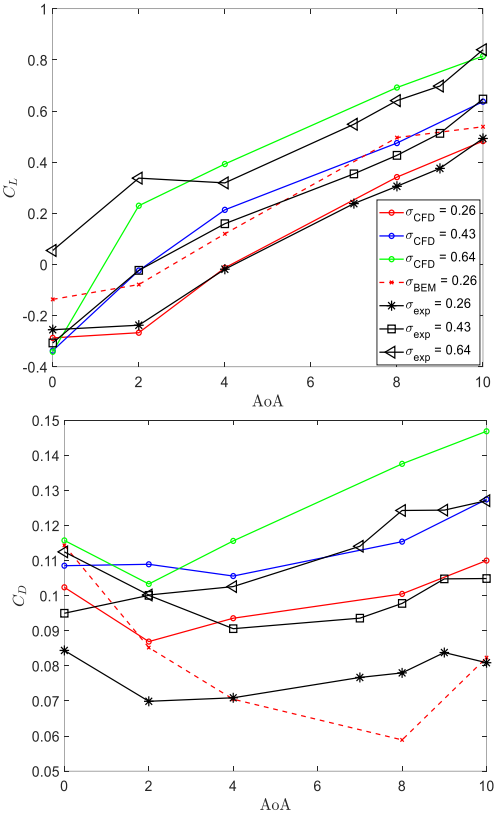

Figure 10. Variation in performance parameters with respect to AoA. Black lines indicate experimental data, colored solid lines indicate CFD data, and colored dotted lines indicate BEM data. $\sigma = 0.26, 0.43$, and 0.64. Top (a) shows the variation in C_L and Bottom (b) shows the variation in C_D

selected based on steady supercavitating, relatively partial cavitation, and unsteady partial cavitation operating conditions. Therefore, the average cavitation numbers of the different operating conditions considered are 0.26 ± 0.02, 0.43 ± 0.02, and 0.64 ± 0.08. The angle of attack is 10^o and the unsteady RANSE model considered used the $k-\omega$ turbulence model with the full Rayleigh Plesset cavitation model. These simulations used σ_v. The BEM predictions were also analyzed and used σ_k.

Figure 10 (a) compares the predicted C_L from the CFD simulation and the BEM with the experimental data. At low cavitation numbers, there is a very good agreement between the unsteady RANSE data and the experimental data. On the other hand, the BEM overpredicts the C_L by a near constant value throughout the range of angles of attack. At higher σ values, there is good agreement between the unsteady RANSE predictions and the experimental C_L at large angles of attack. At low angles of attack, the simulation predictions and experimental data show a discrepancy. Lastly, at higher σ values where partial and unsteady cavitation occurs, the BEM predictions produced invalid results. The BEM assumes a steady cavitation. Due to this, its accuracy in predictions is limited to supercavitating conditions.

Figure 10 (b) compares the predicted C_D values from the CFD simulation and the BEM with the experimental data. It can be observed that regardless of the cavitation number, the unsteady RANSE simulation overpredicts C_D. Neither the predictions from the CFD simulation nor the BEM agree with the experimental data.

Further investigation revealed that despite its limitations, the $k-\omega$ turbulence model and the full Rayleigh-Plesset cavitation model resulted in the most accurate performance predictions even across a range of angles of attack. However, as seen in Fig. 9, the cavitation pattern predicted by this combination of models is not accurate.

8 INFLUENCE OF SEED DENSITY AND SEED DIAMETER

The seed density and seed diameter of the multiphase material in experimental and computational environments play a significant role in determining the nature of cavitation. At $\sigma = 0.444$ and AoA = 10^o, the influence of seed density and seed diameter on the cavitation patterns was assessed for an unsteady RANSE simulation using the $k-\omega$ turbulence model and the full Rayleigh-Plesset cavitation model. All previous analyses were conducted at a seed density and seed diameter of 10^{12} m^{-3} and 10^{-6}m, respectively. It is important to note that this analysis was also conducted on the simulation using a $k-\epsilon$ turbulence model with a Schnerr-Sauer cavitation model. The variation of the control parameters showed similar influences on the shape of the cavitation bubble to a certain extent after which an increase in seed density caused the simulation to collapse. Further investigation needs to be performed to determine the criteria for such a scenario.

8.1 Varying the Seed Density

The seed density is varied systematically between 10^{11} m^{-3} and 10^{14} m^{-3}. As the seed density increased, the cavitation prediction from the unsteady RANSE simulation became more comparable to the experimental images in Figure 4. This can be observed in Figure 11 (b) which shows the cavitation pattern observed with a seed density of 7.5×10^{13} m^{-3}. This can be compared to Fig. 11 (a) which had a seed density of 10^{12} m^{-3}. It is important to note that while these figures are instantaneous images, the cavitation bubble is unsteady. Furthermore, as the seed density increased, C_L increased by 9.68% and C_D increased by 13.86%. Further investigation is required to determine the cause of this variation in forces.

8.2 Varying Seed Diameter

The seed diameter used in the CFD simulations is systematically varied between 10^{-4}m and 10^{-7}m. The seed density was kept constant at 10^{12}. Figures 12 (a) and (b) show the cavitation patterns predicted using a seed

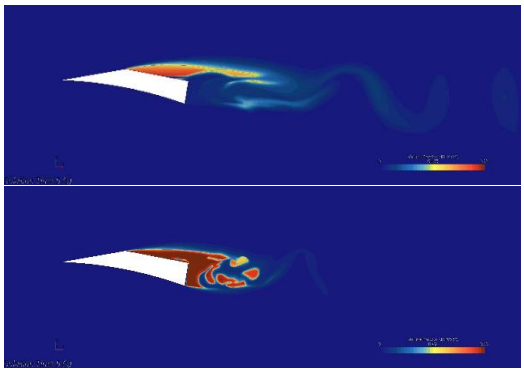

Figure 11. Influence of seed density on cavitation patterns predicted by unsteady RANSE simulation using $k-\omega$ turbulence model and full Rayleigh-Plesset cavitation model. $\sigma = 0.444$ and AoA = 10^o. Warmer regions represent vapor. Top (a): Cavitation pattern observed with seed density = 10^{12}. Bottom (b): Cavitation pattern observed with seed density = $7.5 \times 10^{13}\ m^{-3}$.

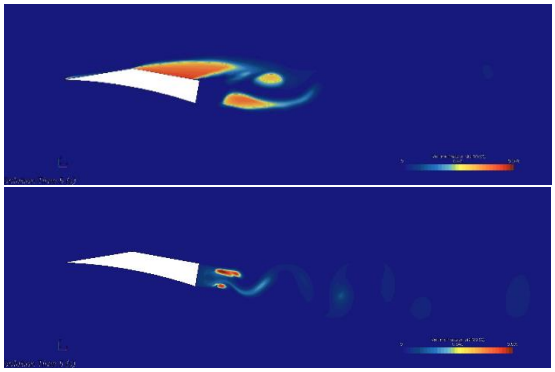

Figure 12. Influence of seed diameter on cavitation patterns predicted by unsteady RANSE simulation using $k-\omega$ turbulence model and full Rayleigh-Plesset cavitation model. $\sigma = 0.444$ and AoA = 10^o. Warmer regions represent vapor. Top (a): Cavitation pattern observed with seed diameter = 10^{-4}m. Bottom (b): Cavitation pattern observed with seed diameter = 10^{-7}m.

diameter of 10^{-4}m and 10^{-7}m, respectively. These are instantaneous images but once again it is important to note that the cavitation bubble is unsteady. As the seed diameter increased, the cavitation pattern predicted by the CFD model improved. As the seed diameter decreases, C_L increases by 81% at 10^{-7}m and C_D decreased by 1.92%. This seed diameter was the only setting that demonstrated such an extreme change in forces which otherwise remained almost constant. Further investigation is required to determine the cause of this variation in forces.

9 CONCLUSIONS

A systematic study was conducted to quantify the uncertainty associated with performance predictions and cavitation pattern predictions from various unsteady RANSE models and numerical approaches. The simulations were two phased and 2D in nature. Various physics models were utilized to simulate the flow conditions. Numerical predictions were also made using a low order, potential based, 2D BEM. The RANSE and potential based predictions were validated against experimental data. The Circular Arc Hydrofoil performance data from Parkin (1956) was used for this.

The analysis conducted indicated that simulating cavitating flow with $k-\omega$ turbulence model and full Rayleigh-Plesset cavitation model produced the most accurate performance predictions. This was found to be true especially at low cavitation numbers and across various angles of attack. On the other hand, simulations using the $k-\epsilon$ turbulence model and the Schnerr-Sauer cavitation model demonstrated the most accurate predictions for cavitation patterns. The BEM results also showed good agreement with the experimental data. However, this was limited to low cavitation numbers as the method is not suitable for unsteady cavitating conditions. In this study, that range is $\sigma > 0.6$. For example, when AoA = 10^o, the percentage difference between the experimental and BEM C_L data sets was found to be ranging from 6.8% to 16.4%. Additionally, the cavitation pattern predictions by the BEM were also found to be accurate in terms of cavitation shape and locations on the SCH section. The BEM predictions were obtained using significantly fewer resources as compared to the unsteady RANSE simulations. It was found that across all approaches, C_L predictions were more accurate than C_D predictions.

Further investigation into the influence of seed density and seed diameter on the cavitation pattern predictions revealed that as the seed density and diameter increases, the cavitation pattern improves. Deeper investigation is required to determine the exact parameters needed to simulate the experimental operating conditions and more accurately predict the cavitation patterns.

Other future works include:

- Quantifying the uncertainty for LES and DES simulations in 3D by validating them against experimental data.
- Quantifying the uncertainty of unsteady RANSE and numerical predictions for more practical and realistic hydrofoil geometries or propeller sections both in 2D and 3D.
- Further investigating the influence of model control parameters on cavitation performance and pattern predictions.
- Extending the performance prediction capabilities of the 2D BEM in the wake for improved drag and cavitation extent predictions.

REFERENCES

Fine, N. E. (1992). 'Nonlinear Analysis of Cavitating Propellers in Nonuniform Flow'. PhD thesis, Department of Ocean Engineering, Massachusetts Institute of Technology.

Fine, N. E., & Kinnas, S. A. (1993). 'A Boundary Element Method for the Analysis of the Flow Around 3-D Cavitating Hydrofoils'. Journal of Ship Research, 37, 3, pp. **213-224**.

Gaggero S, Brizzolara, S. (2008). 'A potential panel method for the prediction of midchord face and back cavitation'. 6th International conference on High Performance Marine Vehicles, vol. 1, **33-46**.

Gaggero, S, Brizzolara, S. (2009). 'A Panel Method for Trans-Cavitating Marine Propellers'. In: Proc. of 7th International Symposium on Cavitation, CAV2009. Ann Arbor (MI), August 2009, vol: **12-27**, ISBN: 978-1-61782-642-9

Kinnas, S. Fine, N. (1992). 'A nonlinear boundary element method for the analysis of unsteady propeller sheet cavitation'. In: Nineteenth Symposium on Naval Hydrodynamics, pp.**717-737**.

Matsuda, N. et al. (1994). 'Experimental investigation into the performance of supercavitation propellers'. Papers of Ship Research Institute 31(5).

Parkin, B. R. (1956). 'Experiments on Circular Arc And Flat Plate Hydrofoils in Noncavitating and Full Cavity Flows'. Department of the Navy Bureau of Ships Contract ~ Nonr -220(12).

Tulin, M.B. (1962). 'Supercavitating propellers – history, operating characteristics, mechanisms of operation'. In Fourth Symposium on Naval Hydrodynamics, pp. **239-286**.

Vernengo G., Bonfiglio L., Gaggero S., Brizzolara S. (2016). 'Physics-Based Design by Optimization of Unconventional Supercavitating Hydrofoils'. Journal of Ship Research, 60(4):**1–16**. http://dx.doi.org/10.5957/JOSR.60.4.150074

Young, Y.L. (2002). 'Numerical modeling of supercavitating and surface-piercing propellers'. PhD thesis, University of Texas at Austin.

Young, Y. L., and Kinnas, S. A. (2003b). 'Numerical modeling of super-cavitating propeller flows', Journal of Ship Research, 47, 1, pp. **48-62**.